Journal Title
XX(X):2–??

Reprints and permission:
sagepub.co.uk/journalsPermissions.nav
DOI: 10.1177/ToBeAssigned
www.sagepub.com/
SAGE

Reliability-based topology optimization of piezoelectric smart structures with voltage uncertainty

Bo Yang[1], Changzheng Cheng[1], Xuan Wang[1,2], Zeng Meng[1,2] and Abbas Homayouni-Amlashi[3]

Abstract

Currently, most of the piezoelectric structures are designed under deterministic conditions, where the influence of uncertain factors on the output motion accuracy is ignored. In this work, a probabilistic reliability-based topology optimization method for piezoelectric structure is proposed to deal with the working voltage uncertainty. A nested double-loop optimization algorithm of minimizing the total volume while satisfying the reliability requirement of the displacement performance is established, where the PEMAP-P (piezoelectric material with penalization and polarization) model is used for parameterization of stiffness matrix, piezoelectric coupling matrix and polarization direction. This strategy consists of an inner loop for reliability analysis and an outer loop for topology optimization. The reliability index approach based on most probable point (MPP) is used for realizing the evaluation of reliability constraint in reliability analysis. The sensitivities of reliability constraint with respect to the random variables and design variables are detailed using the adjoint variable method. Typical examples are performed to illustrate the effectiveness of the proposed RBTO method. A comparison of the optimization results for different reliability indexes, standard deviations of the voltage, spring stiffnesses and displacement limits are conducted, as well as the deterministic topology optimization results.

Keywords

reliability-based topology optimization (RBTO), reliability index, piezoelectric structure, uncertainties

Introduction

The piezoelectric effect is a special physical property involving the interconversion between mechanical and electrical energy. Piezoelectric effect can be classified into the direct piezoelectric effect and the inverse piezoelectric effect. The direct piezoelectric effect refers to the piezoelectric material producing an electric field by being subjected to an external load, and the inverse piezoelectric effect refers to the piezoelectric material generating a mechanical deformation when a voltage is applied. The utilization of the inverse piezoelectric effect for piezoelectric materials has attracted significant interest in recent years with the aim of providing an ideal displacement to drive or position. Smart structures made of piezoelectric materials have many advantages including fast response, high displacement resolution, low power consumption, large output force. These advantages make the piezoelectric smart structures widely use in precision-positioning systems or precision-driving devices such as machine tools (Stöppler and Douglas 2008), piezoelectric relay (Mitsuhashi et al. 1985), micro-electromechanical systems (MEMS) (Conway et al. 2007; Rao et al. 2019) and atomic force microscopes (Croft et al. 2001).

The performance of piezoelectric smart structures is significantly dependent on the deformation accuracy of piezoelectric materials. However, since piezoelectric materials are non-centrosymmetric crystals, the working stroke is only a limited distance and is usually insufficient. This hinders further development of the piezoelectric smart structures. In order to mitigate this issue, various approaches have been developed to improve the efficiency of piezoelectric materials in piezoelectric smart structures. Early optimization research of piezoelectric smart structures focused on the placement and size of the piezoelectric actuators (Frecker 2003). Hać and Liu (1993) proposed a systematic methodology based on the controllability and observability gramians to determine the location of actuators and sensors for a simply supported beam and a rectangular plate. Han and Lee (1999) used genetic algorithms to search the optimal locations of both piezoelectric sensors and actuators based on controllability, observability and spillover prevention in smart composite structures. Suleman and Gonicalves (1999) proposed a multi-objective optimization approach based on the Heaviside function for an adaptive composite beam, which determines not only the position but also the size of the piezoelectric actuator. It can be noted that all of the optimizing works mentioned above assume that host structures and piezoelectric actuators are predetermined, which gives a topology restriction to the optimizing problems. Therefore, the design of free topological distribution of piezoelectric materials or host structure materials has become a hot research topic.

[1,] Department of Engineering Mechanics, Anhui Key Laboratory of Civil Engineering Structures and Materials, Hefei University of Technology, Hefei 230009, China
[2] State Key Laboratory of Reliability and Intelligence of Electrical Equipment, Hebei University of Technology, Tianjin 300401, China
[3] FEMTO-ST Institute, Department AS2M, Université Bourgogne Franche-Comté, 24 Rue Alain Savary, Besancon, France

Corresponding author:
Changzheng Cheng and Xuan Wang, Department of Engineering Mechanics, Anhui Key Laboratory of Civil Engineering Structures and Materials, Hefei University of Technology, Hefei 230009
Email: changzheng.cheng@hfut.edu.cn, xuanwang@hfut.edu.cn

Topology optimization (Bendsøe and Kikuchi 1988; Bendsøe 1989) is an efficient technology dealing with material distribution. Based on topology optimization techniques, many approaches have been greatly developed for the design of piezoelectric smart structures. Silva et al. (1997) first applied the topology optimization method based on homogenization theory to piezoelectric materials, which improved the performance characteristics of two-dimensional plane strain microstructure. However, they only considered the eigenfrequency of a periodic unit cell, not the efficiency of the inverse piezoelectric effect. Silva (1999) proposed a classical interpolation model of piezoelectric materials to design piezoelectric transducers consisted of a flexible mechanical structure and a stack of piezoceramics for maximizing the output displacement (or force) in some specified direction. Frecker and Canfield (2000) introduced predefined ground structures of both truss and frame elements to design a compliant mechanical amplifier for piezoceramic stack actuators by removing useless elements. Silva et al. (2000) presented a general approach based on the homogenization method to design flextensional compliant coupled to the piezoceramic under the placement and topology of the actuator are predetermined, which can maximize the output displacement. Silva (2003) proposed a general method based on topology optimization to design systematically a flexible structure for a linear piezoelectric motor, where quasistatic or low-frequency applications are considered. However, these studies have focused on the amplification of the output force or displacement for a fixed stacked actuator by a compliant mechanism. This is better than size and placement optimization of actuators, but still does not fully exploit the advantages of topology optimization. To further improve the performance of piezoelectric structures, researches of smart structures composed of pure piezoelectric materials or embed with piezoelectric actuators have also been developed. Buehler et al. (2004) developed a new unit cell by combining smart (piezoelectric) and conventional materials through the homogenization technique to maximize the deflection of any node of the structures. Kögl and Silva (2005) extended the conventional PEMAP (piezoelectric material with penalization) model based on the density method by adding a new design variable that describes the polarization of the piezoelectric material, for solving the piezoelectric actuators problems. Zheng et al. (2007) proposed introducing a new electrode density based on the SIMP method for the design of maximizing out-displacement of the piezoelectric actuator. Kang and Tong (2008) proposed a topology optimization for the integrated optimization of structural layout and control voltage of piezoelectric laminated plates using the material density method. Luo et al. (2009) presented an indicator function formulated by several piecewise constants based on the level set method for shape and topology optimization of compliant piezoelectric actuators with the in-plane motion. Kang et al. (2011) presented a mathematical formulation that took the actuator voltage applied on piezoelectric material into account and simultaneously optimized the layouts of the piezoelectric material and the conventional material, as well as the actuation voltage. Wang et al. (2014) employed the level set function to describe the geometrical shapes and placement of the piezoelectric actuators for optimizing the positions of the movable actuators and the topology of the host structure based on independent point-wise density interpolation (iPDI) approach. Schlinquer et al. (2020) designed a piezoelectric actuator by topology optimization combining both piezoelectric material expansion and compression when the voltage condition imposed to each plane-stress element was the same and performed experiments to validate the obtained designs. However, while the working strokes of piezoelectric smart structures have been extended successfully through the introduction of topology optimization, so far the uncertainty of the overall structures has been completely neglected.

Reliability-based design optimization (RBDO) (Cornell 1969; Youn et al. 2005; Meng et al. 2020) integrates design optimization and reliability analysis under various uncertainties for engineering structure. Maute and Frangopol (2003) introduced the concept of RBDO to topology optimization technique, resulting in the so-called reliability-based topology optimization (RBTO). By this RBTO method, they designed the reliable force inverter mechanisms accounting for uncertainties in material properties and load conditions. Zhang and Ouyang (2008) presented a level set methodology for the design of multiple inputs and outputs compliant mechanisms considering the uncertainties of the loads, material properties, and member geometries. A recent work (Wang et al. 2019) provided a reliable design of compliant mechanisms considering interval uncertainties. In these works, the design of compliance mechanisms considering uncertainty factors is based on isotropic materials. However, it should be emphasized that uncertainties such as geometric variation and load magnitude are equally inevitable in piezoelectric smart structures. Whereupon, researchers begin to focus on the optimization problem of piezoelectric smart structures considering uncertainty. Based on the reliability analysis of Monte Carlo simulation method, Franco and Varoto (2012) applied multi-parameter Sequential Quadratic Programming (SQP) optimization technique to the stochastic design of a beam type piezoelectric energy harvesters. Seong et al. (2017) proposed a reliability-based design optimization method for designing a reliable energy harvester satisfying the target reliability on power generation. Wan et al. (2020) developed a new ensemble modeling approach of RBDO for the flexure-based bridge-type amplification mechanisms. It should be noted that most of the existing studies of piezoelectric smart structures are based on the framework of reliability-based design optimization, which is frequently applied to sizing and shape optimization. To the best of our knowledge, there is only one work to integrate RBDO into the topology optimization of piezoelectric smart structures. Sadeghbeigi Olyaie et al. (2013) introduced an optimum finite method into the reliability-based topology optimization of a linear piezoelectric micromotor, where the velocity at the beam endpoint of the suggested micro-motor is maximized. But this study only considers the material distribution, completely ignoring the impact of polarization direction. Considering polarization direction optimization can result in piezoelectric smart structures with improved motion performance, allow piezoelectric materials to realize expansion and compression deformation in the same plane with the same voltage condition. In addition, higher motion gains could be applied to piezoelectric smart structures without exceeding a maximum voltage condition. It is necessary to propose an RBTO method based on multi-parameters optimization for piezoelectric smart structures, which satisfies the target reliability on output displacement with considering the uncertainty factors.

In this study, we propose an RBTO method of piezoelectric smart structures with multi-parameters optimization based on the author's previous work (Homayouni-Amlashi et al. 2020). The proposed approach embeds reliability analysis into the entire topology optimization process, providing a proper design that meets reliability requirements. The uncertainty of operation voltage is considered in the reliability analysis using the Hasofer-Lind and Rackwitz-Fiessler (HL-RF) recursive algorithm. This study considers not only the piezoelectric material distribution but also the configuration of polarization direction. Topology configuration and electrode direction are simultaneously optimized to gain their mobility from the flexibility of their structures. Three numerical examples are performed to illustrate the effectiveness of the proposed RBTO method for design problem of piezoelectric smart structures considering voltage uncertainty.

Finite element analysis of piezoelectric structure

In this paper, the linear constitutive relation is formulated for describing the piezoelectric material by neglecting thermal coupling. It reads (Zheng et al. 2009)

$$\begin{Bmatrix} \mathbf{T} \\ \mathbf{D} \end{Bmatrix} = \begin{bmatrix} \mathbf{c}^E & -\mathbf{e} \\ \mathbf{e}^t & \boldsymbol{\varepsilon}^S \end{bmatrix} \begin{Bmatrix} \mathbf{S} \\ \mathbf{E} \end{Bmatrix} \tag{1}$$

where $\mathbf{T}$ and $\mathbf{S}$ are the vectors of mechanical stresses and strains. $\mathbf{E}$ is the vector of electric field. $\mathbf{D}$ is the vector of dielectric displacement. $\mathbf{c}^E$ is the mechanical stiffness matrix for constant electric field $\mathbf{E}$. $\boldsymbol{\varepsilon}^S$ is the permittivity matrix for constant mechanical strain $\mathbf{S}$. $\mathbf{e}$ is the piezoelectric matrix and the superscript t means transposed.

The optimization model considered here is a thin piezoelectric plate sandwiched symmetrically between two electrode plates, as shown in Fig.1. To produce only mechanical deformation in the plane, the piezoelectric plate has the polarization direction parallel to the z direction. Neglecting the thickness of electrode plates, a plane stress model for the piezoelectric plate is employed in this study. According to plane-stress assumption, the constitutive relation of the piezoelectric layer can be expressed as (Junior et al. 2009)

$$\begin{bmatrix} T_1 \\ T_2 \\ T_6 \\ D_3 \end{bmatrix} = \begin{bmatrix} c_{11}^* & c_{12}^* & 0 & -e_{31}^* \\ c_{12}^* & c_{11}^* & 0 & -e_{31}^* \\ 0 & 0 & c_{66}^* & 0 \\ e_{31}^* & e_{31}^* & 0 & \varepsilon_{33}^* \end{bmatrix} \begin{bmatrix} S_1 \\ S_2 \\ S_6 \\ E_3 \end{bmatrix} \tag{2}$$

where e_{ij}^* , c_{ij}^* and ε_{ij}^* are the piezoelectric coupling constants, stiffness constants and permittivity constants. The values of these constants can be obtained from Junior et al. (2009).

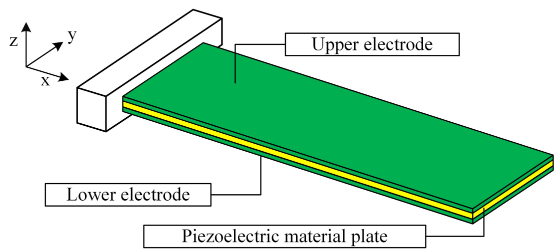

Figure 1. Schematic diagram of a piezoelectric cantilever sandwiched between electrodes

Now, the finite element analysis model should be constructed. The piezoelectric layer is discretized by four nodes square finite elements. The number of mechanical degrees of freedom of each node of the element is 2, respectively in the x direction and y direction. Since the piezoelectric material plate is covered by two fully conductive electrodes, one electrical degree of freedom is adequate to simulate the electrical response of an element. Hence, the strain and electrical field of a single element can be expressed by shape functions as (Lerch 1990)

$$\boldsymbol{S}^e = \boldsymbol{B}_u \boldsymbol{u}^e \tag{3}$$

$$\boldsymbol{E}^e = \boldsymbol{B}_\phi \boldsymbol{\phi}^e \tag{4}$$

Here, $\boldsymbol{u}^e$ and $\boldsymbol{\phi}^e$ are respectively mechanical displacement vector and electric potential value of a single element. $\boldsymbol{B}_u$ and $\boldsymbol{B}_\phi$ are respectively the mechanical and electrical gradient matrices related to the derivative of shape functions. Since the electric potential is assumed to vary linearly between two electrode plates, the strain matrix is $\boldsymbol{B}_\phi = 1/h$ (Junior et al. 2009), where h is the thickness of the piezoelectric plate.

By using the Virtual Work Principle (VWP), above equations and assembling the contributions of all the finite elements, the linear expression of 2D global finite element for piezoelectric material is written as

$$\begin{bmatrix} \mathbf{K}_{uu} & \mathbf{K}_{u\phi} \\ \mathbf{K}_{\phi u} & -\mathbf{K}_{\phi\phi} \end{bmatrix} \begin{bmatrix} \boldsymbol{u} \\ \boldsymbol{\phi} \end{bmatrix} = \begin{bmatrix} \boldsymbol{F} \\ \boldsymbol{Q} \end{bmatrix} \tag{5}$$

where $\boldsymbol{u}$ denotes the global vector of displacement. $\boldsymbol{\phi}$ denotes the global vector of electrical potential. $\boldsymbol{F}$ denotes the global vector of imposed force. $\boldsymbol{Q}$ is the external charge. $\mathbf{K}_{uu}$ and $\mathbf{K}_{\phi\phi}$ are respectively the global mechanical stiffness matrix and global dielectric matrix. $\mathbf{K}_{u\phi}$ and $\mathbf{K}_{\phi u}$ are the global piezoelectric coupling matrices with $\mathbf{K}_{u\phi} = \mathbf{K}_{\phi u}^T$.

Unlike the conventional structures stimulated by an external load, the piezoelectric plate is actuated by the inverse piezoelectric effect. Thus, the external force $\boldsymbol{F}$ is null and the voltage imposed on the electrodes is considered to be an external input. The displacement performance of the piezoelectric plate is the focus of this study so that the second relation of Eq. (5) is ignored in the optimization process. Hence, the global equilibrium equation of the piezoelectric plate can now be rewritten as

$$\mathbf{K}_{uu}\boldsymbol{u} + \mathbf{K}_{u\phi}\boldsymbol{\phi} = 0 \tag{6}$$

Notice there exists a huge scale difference between mechanical stiffness matrix ($\mathbf{K}_{uu}$) and dielectric matrix ($\mathbf{K}_{u\phi}$) in Eq. (6), which may generate numerical singularity in the finite element analysis. To avoid this problem and ensure the accuracy of displacement response, normalization method is adopted as the author's previous work in (Homayouni-Amlashi et al. 2020). The normalization mechanical stiffness matrix and the normalization piezoelectric coupling matrix are expressed as follows

$$\tilde{\mathbf{K}}_{uu} = \frac{1}{k_0}\sum_{i=1}^{NE}\mathbf{K}_{uu}^e, \quad \tilde{\mathbf{K}}_{u\phi} = \frac{1}{\alpha_0}\sum_{i=1}^{NE}\mathbf{K}_{u\phi}^e \tag{7}$$

where k_0 and α_0 are the highest values of each element matrix. NE is number of elements used to discretize the piezoelectric plate. $\mathbf{K}_{uu}^e$ and $\mathbf{K}_{u\phi}^e$ are the mechanical stiffness matrix and the dielectric stiffness matrix for element, respectively, which can be defined as

$$\mathbf{K}_{uu}^e = \int_{A^e} \boldsymbol{B}_u^t \boldsymbol{c}^E \boldsymbol{B}_u dxdy, \quad \mathbf{K}_{u\phi}^e = \int_{A^e} \boldsymbol{B}_u^t \boldsymbol{e} \boldsymbol{B}_\phi dxdy \tag{8}$$

Then, substituting Eq. (7) into Eq. (6), the global finite element equation in normalized form for in-plane motion can be written as

$$k_0\tilde{\mathbf{K}}_{uu}\boldsymbol{u} + \alpha_0\tilde{\mathbf{K}}_{u\phi}\boldsymbol{\phi} = 0 \Rightarrow \tilde{\mathbf{K}}_{uu}\tilde{\boldsymbol{u}} + \tilde{\mathbf{K}}_{u\phi}\boldsymbol{\phi} = 0 \tag{9}$$

Here, $\tilde{\boldsymbol{u}}$ is the normalized displacement vector, which is formed by $\tilde{\boldsymbol{u}} = \frac{k_0}{\alpha_0}\boldsymbol{u}$.

Reliability-based topology optimization

In this work, we want to seek the best design of a piezoelectric smart structure that meets the constraint for reliability. The emphasis is to combine RBDO and topology optimization, resulting in reliability-based topology optimization (RBTO). To show the forming process of RBTO, we first introduce the RBDO problem and reliability evaluation. Then, a PEMAP-P interpolation model based on density distribution is applied. Finally, the formulation of reliability-based topology optimization for piezoelectric structures is presented.

Foundation formula for RBDO

It is widely recognized that engineering design should account for the stochastic nature of engineered systems. Reliability-based design optimization (RBDO) integrates design optimization and reliability analysis under various uncertainties for engineering structure, which makes utilization of failure probability as constraint function to find an optimum design solution that satisfies a given reliability target with respect to performance function. The general mathematical formula for RBDO can be expressed as follows (Youn et al. 2005):

$$\begin{aligned} &\text{minimize} && \mathrm{Cost}\left(\mathbf{d}\right) \\ &\text{subject to} && P_{F_i} = \mathrm{P_r}\left[G_i\left(\mathbf{d},\mathbf{X}\right) \leqslant 0\right] \leqslant P_{F_i}^t \quad i=1,2,...,np \\ &&& \mathbf{d}^L \leqslant \mathbf{d} \leqslant \mathbf{d}^U \end{aligned} \tag{10}$$

where $\mathbf{d}$ denotes the vector of design variable. $\mathbf{X}$ denotes the vector of random variables. P_F denotes the failure probability. P_F^t denotes the failure probability limit. $\mathrm{P}_r\left[\cdot\right]$ denotes the probability operator. $G_i\left(\mathbf{X}\right)$ denotes i-th limit state function used to evaluate the operating state of engineering structure. $G_i\left(\mathbf{X}\right) < 0$ denotes structure failure. np denotes the number of limit state functions. $\mathbf{d}^U$ and $\mathbf{d}^L$ denote the upper and lower limit of design variable vector. The probability of failure is defined by a multi-dimensional integration in the failure domain, which can be expressed as (Jung et al. 2020)

$$P_F = F_G\left(0\right) = \int_{\Omega_F=\{\mathbf{X}\in\mathbb{R}^N:G(\mathbf{X})\leqslant 0\}} f_{\mathbf{X}}\left(\mathbf{X}\right) d\mathbf{X} \tag{11}$$

where $F_G\left(\cdot\right)$ is the cumulative distribution function (CDF). $f_{\mathbf{X}}\left(\mathbf{X}\right)$ is the joint probability density function (PDF) of the random variable vector $\mathbf{X}$. However, it is often very difficult to get joint probability density function and evaluate the multi-dimensional integral of Eq. (11) in engineering practice. Therefore, many approximate probability integration methods have been proposed to provide efficient solutions, such as the most probable point (MPP)-based methods (e.g. the first order reliability method (FORM) and the second order reliability method (SORM)), sampling methods (e.g. the Monte Carlo simulation and importance sampling) and stochastic response surface methods. In general, the value of failure probability limit P_F^t in Eq. (11) should be less than $10^{-3} - 10^{-5}$. As it is impossible to perform effectively RBTO with small probabilities, a series of practicable approaches has been proposed to prescribe the probabilistic constraint, e.g. reliability index approach (RIA) and performance measure approach (PMA). In this paper, the RBDO problem is founded by the RIA, which describes the probabilistic constraint by a reliability index β. Here, β is the an inverse Gaussian transformation of failure probability ($\beta = -\Phi^{-1}\left(P_F\right)$). Because of its high efficiency and stability, the FORM has a extensive application in the evaluation of the probabilistic constraint in RBDO problem. In FORM, the random variable vector $\mathbf{X}$ in original space should be transformed to the random variable vector $\mathbf{Y}$ in standard normal space by using the Rosenblatt transformation (Jung et al. 2020). The reliability index β is defined as the shortest distance from the origin to the limit state surface in the standard normal space. Therefore, the reliability index β is solved by a constrained optimization problem in the standard normal space (Cheng et al. 2006; Santosh et al. 2006), i.e.

$$\begin{aligned} &\text{minimize} \quad \beta\left(\mathbf{Y}\right)=\sqrt{\left(\mathbf{Y}^T\mathbf{Y}\right)} \\ &\text{subject to} \quad G\left(\mathbf{Y}\right)=0 \end{aligned} \tag{12}$$

Hasofer-Lind and Rackwitz-Fiessler (HL-RF) recursive algorithm is currently the most popular method for solving Eq. (12). The reliability index β in HL-RF iteration algorithm can be updated by the following formula (Hasofer 1974; Cheng et al. 2006)

$$\beta^i=\frac{G\left(\mathbf{Y}^i\right)-\left(\bigtriangledown_{\mathbf{Y}}G\left(\mathbf{Y}^i\right)\right)^T\mathbf{Y}^i}{\left\|\bigtriangledown_{\mathbf{Y}}G\left(\mathbf{Y}^i\right)\right\|} \tag{13}$$

where the superscript i represents the current iteration step. Subsequently, the random variable vector $\mathbf{Y}$ is renewed via the following formula

$$\mathbf{Y}^{i+1}=-\beta^i\frac{\bigtriangledown_{\mathbf{Y}}G\left(\mathbf{Y}^i\right)}{\left\|\bigtriangledown_{\mathbf{Y}}G\left(\mathbf{Y}^i\right)\right\|} \tag{14}$$

PEMAP-P model and density filtering

The design domain is discretized by square finite elements. In a density-based approach, the material distribution of each element is characterized by an pseudo density that can take either the value 0 (void) or 1 (solid material). For conventional isotropic materials, the solid isotropic material with penalization (SIMP) is used to associate the element pseudo density with the Young's modulus. However, piezoelectric materials are non-isotropic materials, and the material characteristic parameters are different in different directions. Therefore, a well-known PEMAP-P interpolation model developed by Kögl and Silva (2005) is used, which relates the element's stiffness matrix and coupling matrix to its density and polarization. The PEMAP-P model is given by

$$\begin{aligned} &\tilde{\mathbf{K}}_{uu}^{e}\left(\tilde{\rho}_e\right)=\tilde{\rho}_e^{p_{uu}}\tilde{\mathbf{K}}_{uu}^{e} \\ &\tilde{\mathbf{K}}_{u\phi}^{e}\left(\tilde{\rho}_e,P_e\right)=\tilde{\rho}_e^{p_{u\phi}}\left(2P_e-1\right)^{p_P}\tilde{\mathbf{K}}_{u\phi}^{e} \end{aligned} \tag{15}$$

where P_e denotes the variable of the element polarization and varies from 0 to 1. $\tilde{\rho}_e$ is the filtered element density, defined by averaging the element densities over a number of elements in a circular region with radius r_{min}. p_{uu}, $p_{u\phi}$ and p_P are penalization coefficients for the stiffness, coupling and polarization values, respectively.

The optimization results in the density-based topology optimization method often suffer from the checkerboard patterns. To obtain a checkerboard-free optimization result, one of the most widely used algorithms is density filtering (Andreassen et al. 2011). Thus, the filtered element density $\tilde{\rho}$ in Eq.(15)

can be expressed as

$$\tilde{\rho}_e = \frac{\sum_{j \in N_i} H_{ej} \rho_j}{\sum_{j \in N_i} H_{ej}} \tag{16}$$

where N_i is a set of elements adjacent to element e. The adjacency relation is defined as $N_i = \{j : \triangle(e, j) \leq r_{min}\}$, here the operator $\triangle(e, j)$ is distance from element j center to element e center. H_{ej} is a weight factor defined as

$$H_{ej} = \max\left(0, r_{min} - \triangle(e, j)\right) \tag{17}$$

Optimization formula for RBTO

This study attempts to minimize the relative volume fraction of piezoelectric structures that meet the displacement reliability constraint under voltage uncertainty. A limit state function (or performance function) with respect to displacement is defined as

$$G(\boldsymbol{\rho}, \mathbf{X}, \boldsymbol{P}) = D_{limit} - D(\boldsymbol{\rho}, \mathbf{X}, \boldsymbol{P}) \tag{18}$$

where D_{limit} is the displacement limit of the appointed output point. D is the displacement of the appointed output point, which can be obtained by $D = -\boldsymbol{L}^T \tilde{u}$. Here, $\boldsymbol{L}$ is a selection vector whose corresponding value is 1 at the appointed output point and 0 at other points. Thus, the RBTO problem based on RIA for piezoelectric structures can be expressed as

$$\begin{aligned} &\text{minimize} \quad V(\boldsymbol{\rho}) = \sum_{e=1}^{NE} \rho_e v_e \\ &\text{subject to} \quad \begin{cases} \tilde{\mathbf{K}}_{uu}\tilde{\boldsymbol{u}} + \tilde{\mathbf{K}}_{u\phi}\boldsymbol{\phi} = 0 \\ \beta_i\left(G(\boldsymbol{\rho}, \mathbf{X}, \boldsymbol{P}) \geq 0\right) \geq \beta_t \quad i = 1, 2, ..., N \\ 0 \leq \rho_e \leq 1 \\ 0 \leq P_e \leq 1 \end{cases} \end{aligned} \tag{19}$$

where NE is the total number of elements used to discretize the design domain. N is the number of constraints. ρ_e and P_e are the density ratio and the polarization direction of the e-th element, respectively. v_e is the volume of each element. β_i represents the HL-RF reliability index, which can be calculated by the HL-RF iterative algorithm. β_t is the required reliability index.

For comparison, the deterministic topology optimization model with volume minimization as the objective function and a specific displacement as the constraint function is also listed herein. The mathematical formulation of deterministic topology optimization can be defined as

$$\begin{aligned} &\text{minimize} \quad V(\boldsymbol{\rho}) = \sum_{e=1}^{NE} \rho_e v_e \\ &\text{subject to} \quad \begin{cases} \tilde{\mathbf{K}}_{uu}\tilde{\boldsymbol{u}} + \tilde{\mathbf{K}}_{u\phi}\boldsymbol{\phi} = 0 \\ G(\boldsymbol{\rho}, \mathbf{X}, \boldsymbol{P}) = D_{limit} - D(\boldsymbol{\rho}, \mathbf{X}, \boldsymbol{P}) \geq 0 \\ 0 \leq \rho_e \leq 1 \\ 0 \leq P_e \leq 1 \end{cases} \end{aligned} \tag{20}$$

The definition of parameters is the same as in Eq. (18) and Eq. (19).

Design sensitivity analysis and solution procedure

Sensitivity analysis is always an important procedure in design optimization. Because the proposed RBTO has two loops: the outer loop for topology optimization and the inner loop for reliability evaluation, the sensitivity analysis for design variables and random variables should be performed, respectively.

Sensitivity analysis for design variables

The design sensitivity of volume objective function is calculated straightly and its calculation is ignored here. Hence, the emphasis of this section is to analyze the sensitivity of the constraint function with respect to design variables. Here the adjoint variable method is used. The Lagrange function for the current reliability index can be expressed as

$$\beta_i(\boldsymbol{\rho}, \boldsymbol{P}) = \frac{D_{limit} + \boldsymbol{L}^T \tilde{\boldsymbol{u}}(\boldsymbol{\rho}, \mathbf{X}, \boldsymbol{P}) - (\triangledown_{\mathbf{Y}} G)^T \mathbf{Y}}{\|\triangledown_{\mathbf{Y}} G\|} + \boldsymbol{\lambda}_\rho^T \left(\tilde{\mathbf{K}}_{uu}(\boldsymbol{\rho}) \tilde{\boldsymbol{u}}(\boldsymbol{\rho}, \boldsymbol{P}) + \tilde{\mathbf{K}}_{u\phi}(\boldsymbol{\rho}, \boldsymbol{P}) \boldsymbol{\phi}\right) \quad (21)$$

The corresponding sensitivity can be written as

$$\begin{aligned} \frac{\partial \beta_i}{\partial \rho_e} &= \frac{\boldsymbol{L}^T}{\|\triangledown_{\mathbf{Y}} G\|} \frac{\partial \tilde{\boldsymbol{u}}}{\partial \rho_e} + \lambda_\rho^T \frac{\partial \left(\tilde{\mathbf{K}}_{uu} \tilde{\boldsymbol{u}} + \tilde{\mathbf{K}}_{u\phi} \boldsymbol{\phi}\right)}{\partial \rho_e} \\ &= \left(\frac{\boldsymbol{L}^T}{\|\triangledown_{\mathbf{Y}} G\|} + \lambda_\rho^T \tilde{\mathbf{K}}_{uu}\right) \frac{\partial \tilde{\boldsymbol{u}}}{\partial \rho_e} + \lambda_\rho^T \frac{\partial \tilde{\mathbf{K}}_{uu}}{\partial \rho_e} \tilde{\boldsymbol{u}} + \lambda_\rho^T \frac{\partial \tilde{\mathbf{K}}_{u\rho}}{\partial \rho_e} \boldsymbol{\phi} \end{aligned} \quad (22)$$

where $\lambda_\rho^T = -\tilde{\mathbf{K}}^{-1} \frac{\boldsymbol{L}^T}{\|\triangledown_{\mathbf{Y}} G\|}$ to remove the $\partial \tilde{\boldsymbol{u}} / \partial \rho_e$ terms. Then, the sensitivity can be calculated as

$$\frac{\partial \beta_i}{\partial \rho_e} = -\tilde{\mathbf{K}}_{uu}^{-1} \frac{\boldsymbol{L}^T}{\|\triangledown_{\mathbf{Y}} G\|} \frac{\partial \tilde{\mathbf{K}}_{uu}}{\partial \rho_e} \tilde{\boldsymbol{u}} - \tilde{\mathbf{K}}_{uu}^{-1} \frac{\boldsymbol{L}^T}{\|\triangledown_{\mathbf{Y}} G\|} \frac{\partial \tilde{\mathbf{K}}_{u\phi}}{\partial \rho_e} \boldsymbol{\phi} \quad (23)$$

Similarly, the design sensitivity with respect to polarization P can be obtained as

$$\frac{\partial \beta_i}{\partial P_e} = -\tilde{\mathbf{K}}_{uu}^{-1} \frac{\boldsymbol{L}^T}{\|\triangledown_{\mathbf{Y}} G\|} \frac{\partial \tilde{\mathbf{K}}_{u\phi}}{\partial P_e} \boldsymbol{\phi} \quad (24)$$

Sensitivity analysis for random variables

Traditionally, the sensitivity for HL-RF method has been assessed by the finite difference method or direct derivation method. Here, we apply the adjoint method to calculate the sensitivity. The limit state function can be rewritten as.

$$G(\boldsymbol{\rho}, \mathbf{X}, \boldsymbol{P}) = D_{limit} + \boldsymbol{L}^T \tilde{\boldsymbol{u}}(\boldsymbol{\rho}, \mathbf{X}, \boldsymbol{P}) + \lambda^T \left(\tilde{\mathbf{K}}_{uu}(\boldsymbol{\rho}) \tilde{\boldsymbol{u}}(\boldsymbol{\rho}, \mathbf{X}, \boldsymbol{P}) + \tilde{\mathbf{K}}_{u\phi}(\boldsymbol{\rho}, \boldsymbol{P}) \boldsymbol{\phi}(\mathbf{X})\right) \quad (25)$$

The corresponding sensitivity can be expressed as

$$\begin{aligned} \frac{\partial G}{\partial \mathbf{X}} &= \boldsymbol{L}^T \frac{\partial \tilde{\boldsymbol{u}}}{\partial \mathbf{X}} + \lambda^T \mathbf{K}_{uu} \frac{\partial \tilde{\boldsymbol{u}}}{\partial \mathbf{X}} + \lambda^T \mathbf{K}_{u\phi} \frac{\partial \boldsymbol{\phi}}{\partial \mathbf{X}} \\ &= \left(\boldsymbol{L}^T + \lambda^T \tilde{\mathbf{K}}_{uu}\right) \frac{\partial \tilde{\boldsymbol{u}}}{\partial \mathbf{X}} + \lambda^T \tilde{\mathbf{K}}_{u\phi} \frac{\partial \boldsymbol{\phi}}{\partial \mathbf{X}} \end{aligned} \quad (26)$$

where $\lambda^T = -\tilde{\mathbf{K}}^{-1}\boldsymbol{L}^T$ to remove the $\partial\tilde{\boldsymbol{u}}/\partial\mathbf{X}$ terms. Eventually, the sensitivity is can be written as follows

$$\frac{\partial G}{\partial \mathbf{X}} = -\tilde{\mathbf{K}}_{uu}^{-1}\boldsymbol{L}^T\tilde{\mathbf{K}}_{u\phi}\frac{\partial \phi}{\partial \mathbf{X}} \tag{27}$$

Solution procedure

Once the design sensitivities with respect to the design variables and random variables are obtained, the method of move asymptotes (MMA) algorithm can be used to solve the RBTO optimization problem in Eq. (19). The outer loop for topology optimization will be terminated when $\max\{|\boldsymbol{\rho}_k - \boldsymbol{\rho}_{k-1}|\} \leqslant 0.001$ or the number of iterations reaches up to 300. The inner loop based on HL-RF method is terminated when $\{|\beta_k - \beta_{k-1}|\} \leqslant 0.001$ is satisfied or 100 iterations is achieved. To clearly show the implementation process, the numerical procedures for the RBTO algorithm of piezoelectric smart structures with voltage uncertainty is shown in Fig. (2).

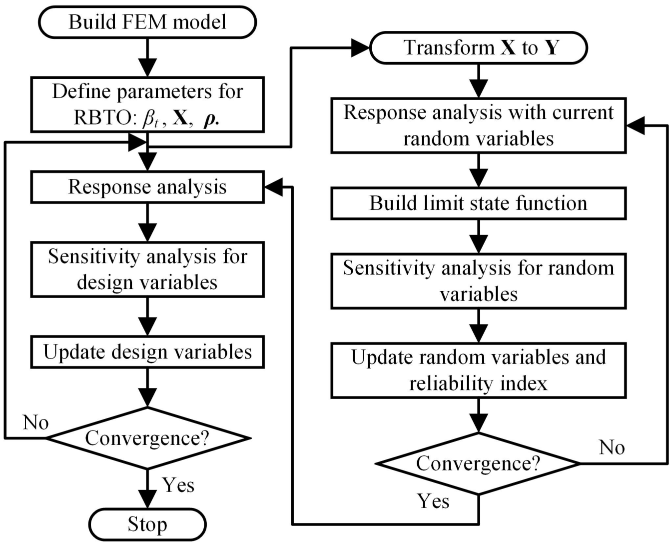

Figure 2. Flowchart of a nested double-loop algorithm for RBTO of piezoelectric smart structures

Design examples and discussions

In this section, several benchmark design examples are performed to illustrate the applicability and validity of the presented RBTO formula for the design problem of piezoelectric smart structures, which includes piezoelectric pusher, piezoelectric gripper and piezoelectric relay. In all the design examples, the parameters for penalization coefficients are $p_{uu} = 3$, $p_{u\phi} = 4$ and $p_P = 1$, and the thickness of piezoelectric plate is 0.1mm. Unless other stated, the initial density of each element is $\rho_e = 1$. The piezoelectric materials used are PZT 4, whose value of properties are presented in Table 1. Additionally, all the voltage imposed on the upper electrode are assumed to obey normal distribution and their means are $\mu = 1$ V. The lower electrode is grounded for all examples. It is notable that displacement response (including D, D_{limit} and $\tilde{u}$) is described by normalized form, which is expressed as a dimensionless value in this paper. The real values of displacement response can be calculated by multiplying the normalized value by α_0/k_0 and the unit is meter. All computation are carried out on an HP laptop equipped with 6 Intel Core i7-9750H 2.6Ghz processors, 16 GB RAM and Windows 10 64-bit operating system.

Table 1. Parameters for PZT 4

Parameter name	Value	Parameter name	Value
c_{11}^*	$9.1187 \times 10^{10}\mathrm{N/m^2}$	c_{66}^*	$3.0581 \times 10^{10}\mathrm{N/m^2}$
c_{12}^*	$3.0025 \times 10^{10}\mathrm{N/m^2}$	e_{31}^*	$-14.9091\mathrm{C/m^2}$

Piezoelectric pusher

As the first example, a well-known piezoelectric pusher with the overall dimension 10 mm$\times$10 mm is considered. The design domain and boundary condition are depicted in Fig.3a. Here, one output point is set on the right edge of the design domain to produce one horizontal displacements D_{out}. To reduce the calculation time, only half of the design domain is considered by making use of the symmetry, as sketched in Fig.3b. The half design domain is discretized into 150$\times$75 plane stress elements. A small artificial spring with stiffness $K_s = 0.01$ is attached to the out point to simulate the workpiece. Besides, the target reliability index β_t and displacement limit D_{limit} in Eq.(18) are set to be 4.00 and -125 respectively.

In this example, the influence caused by different standard deviations ($\sigma = 0.08$ V, 0.10 V, 0.12 V) of voltage is investigated. To show the whole piezoelectric pusher, the obtained results are processed with mirror symmetry. Fig.4 shows the topology configurations and polarization layouts of a typical iteration step for the voltage standard deviation of 0.08 V. It can be seen that the density layouts and polarization profile change smoothly, which means that the proposed method is stable. The final optimization results for different standard deviations of $\sigma = 0.08, 0.10, 0.12$ V are presented in Fig.5. The inner HL-RF loop converges after 3 iterations for different standard deviations. It can be seen from the final results that the density layouts and polarization profile among different voltage standard deviations have obvious differences, which indicates the standard deviations of voltage play an important role in the RBTO of the piezoelectric pusher. It also shows the importance of considering voltage uncertainty in piezoelectric smart structures.

Fig.6 illustrates iterative histories of objective function (i.e., relative volume fraction) for different standard deviations of voltage. It is observed that a stable convergence of the objective function can be obtained, which shows the present method has good stability and repeatability. The volume fraction, reliability index of Monte Carlo simulation and computing cost for different voltage standard deviations are listed in Table 2. 1000000 sample points are selected in the Monte Carlo simulation. From the results of reliability index obtained using Monte Carlo simulation, it is found that the final structure obtained based on the proposed RBTO method can meet the requirements of target reliability relatively well, which means that the proposed method is effective. On the other hand, it can be seen that the relative volume fraction is increased with the increase of standard deviation, which shows that more material is needed to resist the structural insecurity resulting from the rising of standard deviation.

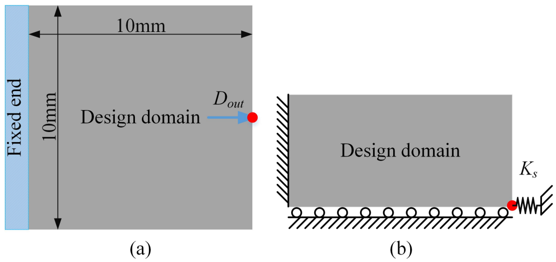

Figure 3. Design domain and boundary condition of piezoelectric pusher

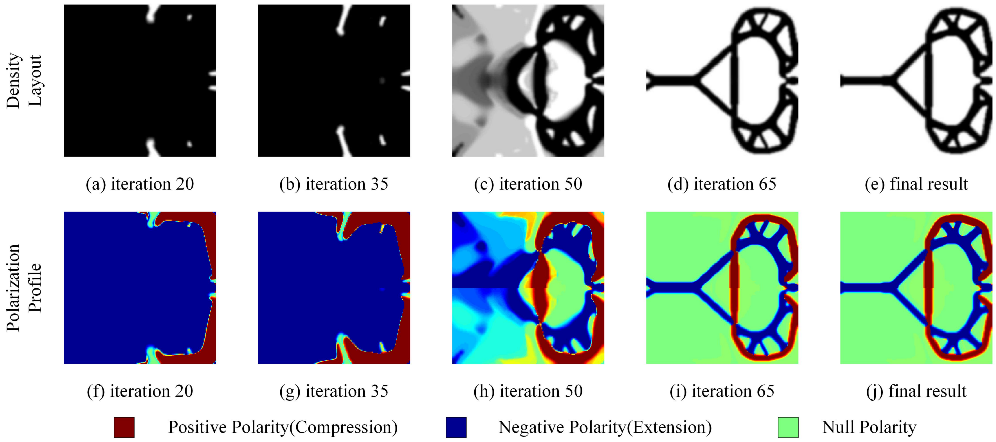

Figure 4. RBTO evolution of piezoelectric pusher with $\sigma = 0.08$ V

Table 2. Comparison of optimization results for DTO and RBTO

Voltage standard deviation	Reliability index of Monte Carlo simulation	Relative volume fraction(%)	Computing time(s)
0.08 V	4.0291	23.02	335.2817
0.10 V	4.0051	28.52	334.7764
0.12 V	4.0051	36.07	338.5953

Piezoelectric gripper

The second example optimized in this paper is a useful piezoelectric gripper with the overall dimension 10 mm$\times$10 mm. The design domain and boundary condition are depicted in Fig.7a. A blank rectangular region of 2 mm$\times$2 mm located on the design domain is treated by passive elements technology (Sigmund 2001) in the optimization. Besides, two output points are set on the bottom to produce two horizontal displacements D_{out}. The half design domain is considered for analysis, as shown in Fig.7b. The half design domain is discretized into 100×50 plane stress elements, in which the densities ρ_e of the passive

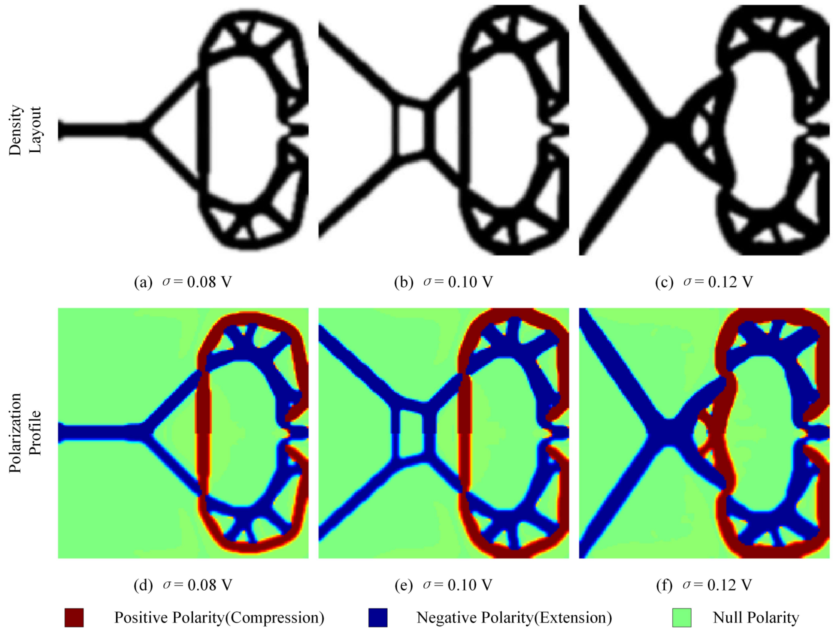

Figure 5. RBTO results of piezoelectric pusher for different voltage standard deviations

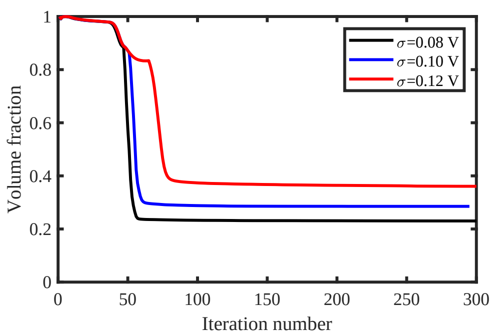

Figure 6. Iterative histories of the volume fraction for different standard deviations

elements of the blank region are set to be 0.001. To simulate the effect of the workpiece, a small artificial spring is introduced and attached to the output point of the piezoelectric gripper. The standard deviation of voltage is set as to $\sigma = 0.10$ V. Additionally, the displacement limit D_{limit} is set to be -105.

To explore the influences of target reliability indexes on the optimization results of the piezoelectric gripper, the values of target reliability indexes are set as $\beta_t = 3.50, 4.00, 4.50$ with spring stiffness $K_s = 0.010$. The traditional deterministic topology optimization (DTO) aimed at minimizing the relative volume fraction under the limit of displacement is also considered for comparison. The same as the above example, the optimization results are symmetrized to represent the entire piezoelectric gripper. Fig.8 and Fig.9 respectively show the optimization results of DTO and RBTO with different target reliability indexes. The inner HL-RF loop converges after 3 iterations for different target reliability indexes. As expected, the density layouts and polarization profiles between DTO and RBTO have significant difference, which shows the importance of considering voltage uncertainties in topology optimization of piezoelectric gripper. The objective function results, reliability indexes and computing time of iterations are listed in Table 3. Here, the reliability index of DTO is calculated by the Monte Carlo method. 100000 sample points are selected in the Monte Carlo simulation. From the data in Table 3, we can obviously see that the larger the reliability index, the larger the volume fraction. That is to say, the improvement of safety usually requires more material consumption.

Additionally, we investigate the RBTO by using different spring stiffness ($K_s = 0.010, 0.012, 0.014$) under the target reliability index $\beta_t = 3.50$. The optimization results are depicted in Fig.10. The inner HL-RF loop converges after 3 iterations for different spring stiffness. By comparing the density layouts of different spring stiffness, we can see that the area of topological configuration increase as the values of spring stiffness increasing. That is, with the increase of the external workpiece effect, the piezoelectric gripper is bound to need more area imposed by the voltage to complete the clamping action. The values of the objective function (34.10%, 39.92% and 46.48%) for different spring stiffness also confirm this view. Besides, the computing time of iterations are 171.1079 s, 173.2706 s and 172.6677 s.

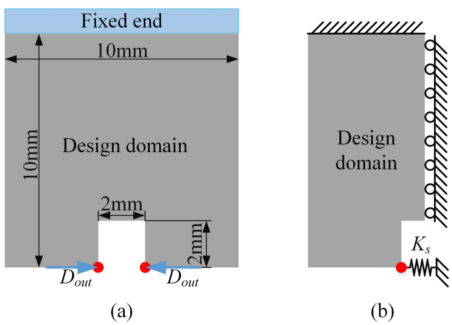

Figure 7. Design domain and boundary condition of piezoelectric gripper

Table 3. Comparison of optimization results for DTO and RBTO

Design method	Reliability index	Relative volume fraction(%)	Computing time(s)
DTO	-0.0328	21.23	83.1816
RBTO	3.50	34.10	171.1079
	4.00	39.22	170.5544
	4.50	46.67	191.0835

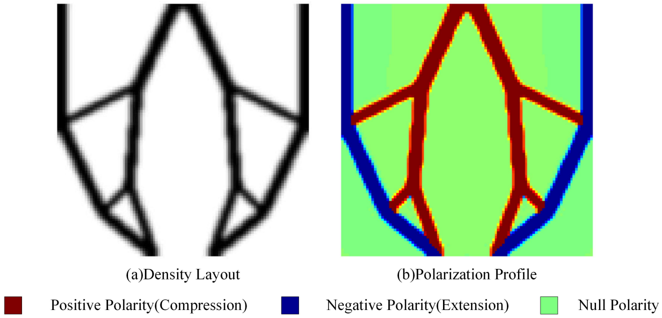

Figure 8. Deterministic topology optimization results of piezoelectric gripper with $D_{limit} = -120$

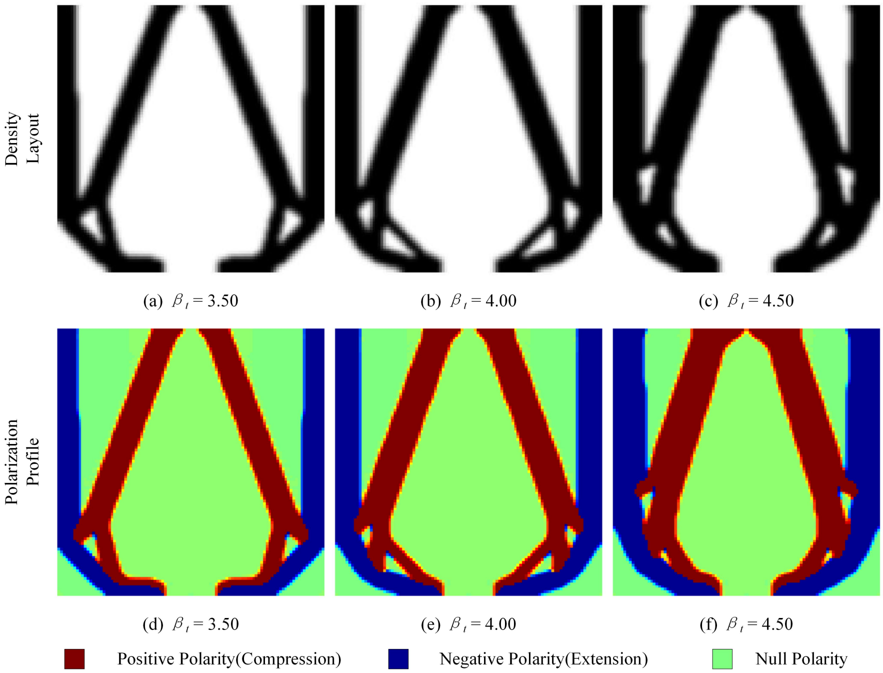

Figure 9. RBTO results of piezoelectric gripper for different target reliability indexes

Piezoelectric relay

In this example, a simple piezoelectric relay with the overall dimension 15 mm$\times$10 mm is optimized. As shown in Fig.11a, a semicircular blank area with a radius of 4 mm is located on the design domain and the down left side of the design domain is fixed. Like the optimization of the piezoelectric gripper, the blank area is formed by passive elements with density $\rho_e = 0.001$. An output point placed at the

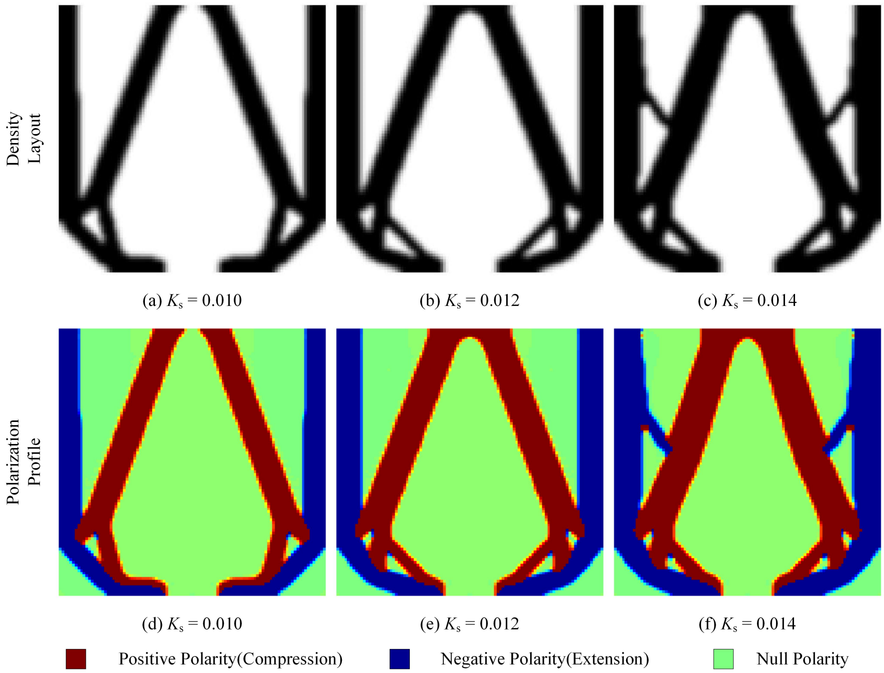

Figure 10. RBTO results of piezoelectric gripper for different spring stiffnesses

lower-right corner is used to produce a vertical displacement D_{out}. To simulate the resistance from the workpiece, a small artificial spring of stiffness $K_s = 0.010$ is linked at the output point, as depicted in Fig.11b. The design domain is discretized with 150×100 standard square plane stress elements. The standard deviation value of voltage is set as 0.10 V.

The first case aims to investigate the influence of displacement limit on the optimization results of the piezoelectric relay. Three different displacement limits ($D_{limit} = -265, -270, -275$) are considered under the target reliability index $\beta_t = 2.00$. The DTO aimed at minimizing the relative volume fraction under the limit of displacement is also carried out for the purpose of comparison. The optimized results of different displacement limits are listed in Fig.12 for DTO and Fig.13 for RBTO. The inner HL-RF loop converges after 2 iterations for different displacement limits. The results of deterministic topology optimization between different displacement limits do not show significant difference in density layouts and polarization profiles. In contrast, however, significant differences can be found in the results of RBTO between different displacement limits. This indicates that the optimization results of piezoelectric relay considering voltage uncertainty are particularly sensitive to changes in displacement limits. The objective function results, reliability indexes and computing time of iterations are listed in Table 4. Here, the reliability index of DTO is calculated by the Monte Carlo method. 100000 sample points are selected in the Monte Carlo simulation. It can be seen from the data in Table 4 that the objective functions for DTO are smaller than RBTO under same displacement limits, which reflects RBTO tends to provide a conservative design compared with DTO.

The second case in this example seek to investigate the impact caused by changes in reliability indexes on optimization of piezoelectric relay. Three different target reliability indexes ($\beta_t = 1.00, 1.50, 2.00$) are considered under the displacement limit $D_{limit} = -270$. Fig.14 shows the optimized result for different target reliability indexes. The inner HL-RF loop converges after 2 iterations for different target reliability indexes. The DTO of $D_{limit} = -270$ in the prior case is applied here for comparison. It should be noticed again that, significant differences in the density layouts and polarization profiles can be observed between DTO and RBTO, as well as RBTO for different target reliability indexes. This well demonstrates the importance of introducing uncertainty factors in the design of piezoelectric smart structures as well as the engineering guidance. Moreover, the objective function, reliability indexes and computing times of iterations for DTO and RBTO are listed in Table 5. The same as the piezoelectric gripper example, the relative volume fraction increases as the reliability index increases. This again illustrates that increased reliability requirements are often accompanied by increased material consumption.

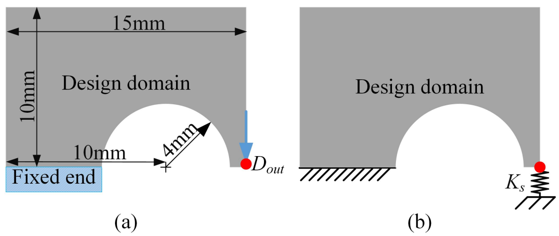

Figure 11. Design domain and boundary condition of piezoelectric relay

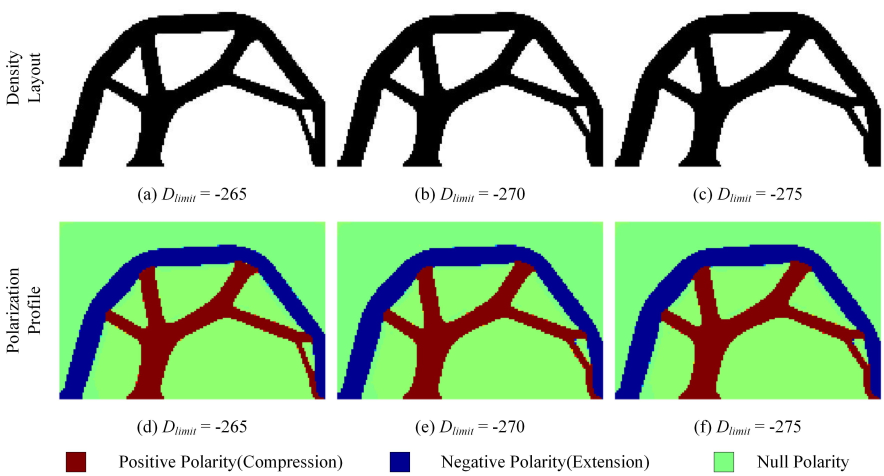

Figure 12. Deterministic topology optimization results of piezoelectric relay for different displacement limits

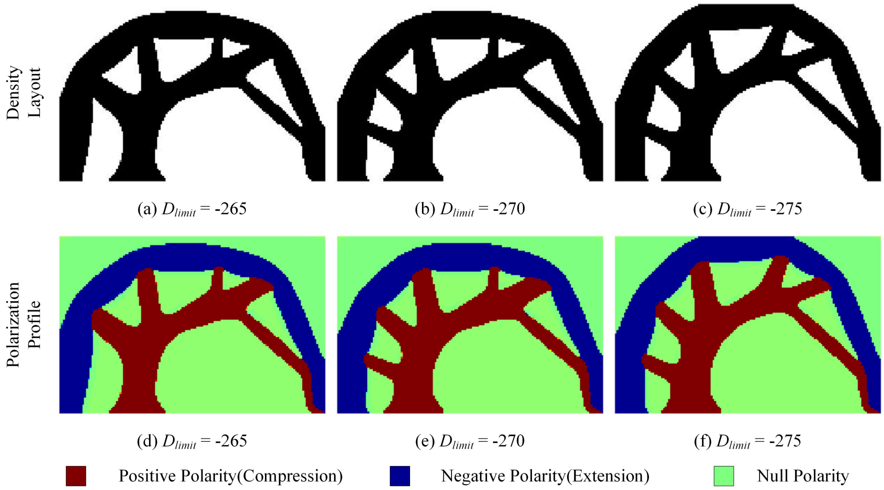

Figure 13. RBTO results of piezoelectric relay for different displacement limits

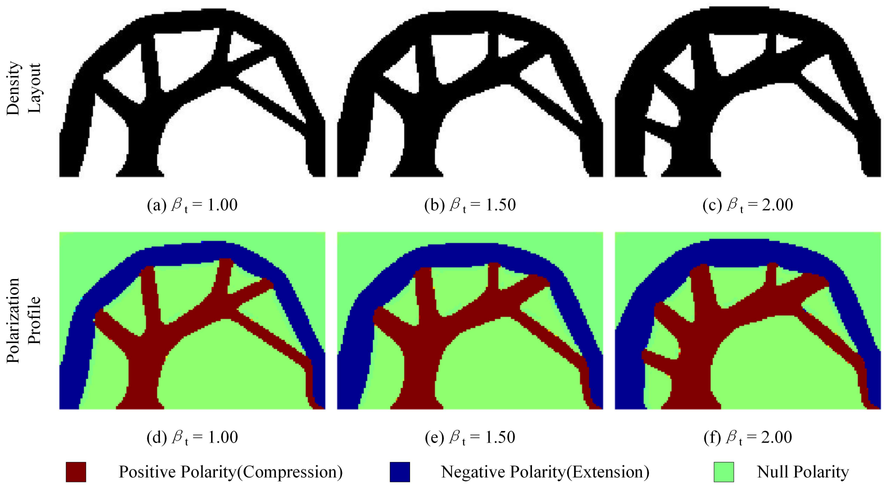

Figure 14. RBTO results of piezoelectric relay for different target reliability indexes

Conclusions

In this research, an efficient reliability-based topology optimization approach is proposed for piezoelectric smart structures with considering the voltage uncertainty. The proposed methodology integrates the RIA-based reliability analysis into the design problem of piezoelectric smart structures, where the PEMAP-P model is used for optimizing the topological configuration and electrode direction simultaneously. Numerical examples show that the displacement-based RBTO design method designs

Table 4. Comparison of optimization results for DTO and RBTO with different displacement limits

Displacement limit	Design method	Reliability index	Relative volume fraction(%)	Computing time(s)
$D_{limit} = -265$	DTO	-0.1840	30.76	246.6350
	RBTO	2.00	45.07	543.2473
$D_{limit} = -270$	DTO	0.0057	31.66	249.4814
	RBTO	2.00	46.83	543.6571
$D_{limit} = -275$	DTO	0.0005	32.59	250.5381
	RBTO	2.00	47.95	542.5252

Table 5. Comparison of optimization results for DTO and RBTO with displacement limit $D_{limit} = -270$

Design method	Reliability index	Relative volume fraction(%)	Computing time(s)
DTO	0.0057	31.66	249.4814
RBTO	1.00	37.97	574.1570
	1.50	41.90	553.2232
	2.00	46.83	543.6571

innovative piezoelectric structures that meet the requirement of given failure probability. The structural layouts and polarization profiles of the piezoelectric smart structures are significantly influenced by the reliability index demands, and the relative volume fraction is increased with the increase of reliability index demands. In addition, compared with deterministic topology optimization, RBTO can provide a more reliable design under the same displacement limit.

Acknowledgements

This work is supported by the Natural Science Foundation of Anhui Province (Grant No. 2008085QA21), the Fundamental Research Funds for the Central Universities (Grant Nos. JZ2020HGTA0080) and the State Key Laboratory of Reliability and Intelligence of Electrical Equipment (Grant No. EERI_KF2020002). These supports are gratefully acknowledged. The authors are also grateful to Prof. Krister Svanberg for providing the procedure of MMA algorithm.

References

Andreassen E, Clausen A, Schevenels M, Lazarov BS and Sigmund O (2011) Efficient topology optimization in matlab using 88 lines of code. *Structural and Multidisciplinary Optimization* 43(1): 1–16.

Bendsøe MP (1989) Optimal shape design as a material distribution problem. *Structural optimization* 1(4): 193–202.

Bendsøe MP and Kikuchi N (1988) Generating optimal topologies in structural design using a homogenization method. *Computer methods in applied mechanics and engineering* 71(2): 197–224.

Buehler MJ, Bettig B and Parker GG (2004) Topology optimization of smart structures using a homogenization approach. *Journal of Intelligent Material Systems and Structures* 15(8): 655–667.

Cheng G, Xu L and Jiang L (2006) A sequential approximate programming strategy for reliability-based structural optimization. *Computers & Structures* 84(21): 1353–1367.

Conway NJ, Traina ZJ and Kim SG (2007) A strain amplifying piezoelectric mems actuator. *Journal of Micromechanics and Microengineering* 17(4): 781–787.

Cornell CA (1969) A probability-based structural code 66(12): 974–985.

Croft D, Shed G and Devasia S (2001) Creep, hysteresis, and vibration compensation for piezoactuators: atomic force microscopy application. *J. Dyn. Sys., Meas., Control* 123(1): 35–43.

Franco V and Varoto P (2012) Parameter uncertainty and stochastic optimization of cantilever piezoelectric energy harvesters. *Proceedings OF ISMA2012* .

Frecker M and Canfield S (2000) Optimal design and experimental validation of compliant mechanical amplifiers for piezoceramic stack actuators. *Journal of Intelligent Material Systems and Structures* 11(5): 360–369.

Frecker MI (2003) Recent advances in optimization of smart structures and actuators. *Journal of Intelligent Material Systems and Structures* 14(4-5): 207–216.

Hać A and Liu L (1993) Sensor and actuator location in motion control of flexible structures. *Journal of sound and vibration* 167(2): 239–261.

Han JH and Lee I (1999) Optimal placement of piezoelectric sensors and actuators for vibration control of a composite plate using genetic algorithms. *Smart Materials and Structures* 8(2): 257–267.

Hasofer AM (1974) An exact and invarient first order reliability format. *J. Eng. Mech. Div., Proc. ASCE* 100(1): 111–121.

Homayouni-Amlashi A, Schlinquer T, Mohand-Ousaid A and Rakotondrabe M (2020) 2d topology optimization matlab codes for piezoelectric actuators and energy harvesters. *Structural and Multidisciplinary Optimization* 63: 1–32.

Jung Y, Cho H and Lee I (2020) Intelligent initial point selection for mpp search in reliability-based design optimization. *Structural and Multidisciplinary Optimization* 62(4): 1809–1820.

Junior CDM, Erturk A and Inman DJ (2009) An electromechanical finite element model for piezoelectric energy harvester plates. *Journal of Sound and Vibration* 327(1-2): 9–25.

Kang Z and Tong L (2008) Integrated optimization of material layout and control voltage for piezoelectric laminated plates. *Journal of Intelligent Material Systems and Structures* 19(8): 889–904.

Kang Z, Wang R and Tong L (2011) Combined optimization of bi-material structural layout and voltage distribution for in-plane piezoelectric actuation. *Computer methods in applied mechanics and engineering* 200(13-16): 1467–1478.

Kim C, Wang S, Rae Kr, Moon H and Choi KK (2006) Reliability-based topology optimization with uncertainties. *Journal of mechanical science and technology* 20(4): 494–504.

Kögl M and Silva EC (2005) Topology optimization of smart structures: design of piezoelectric plate and shell actuators. *Smart materials and Structures* 14(2): 387–399.

Lerch R (1990) Simulation of piezoelectric devices by two-and three-dimensional finite elements. *IEEE transactions on ultrasonics, ferroelectrics, and frequency control* 37(3): 233–247.

Luo Z, Tong L, Luo J, Wei P and Wang MY (2009) Design of piezoelectric actuators using a multiphase level set method of piecewise constants. *Journal of Computational Physics* 228(7): 2643–2659.

Maute K and Frangopol DM (2003) Reliability-based design of mems mechanisms by topology optimization. *Computers & Structures* 81(8-11): 813–824.

Meng Z, Li G, Wang X, Sait SM and Yıldız AR (2020) A comparative study of metaheuristic algorithms for reliability-based design optimization problems. *Archives of Computational Methods in Engineering* : 1–17.

Mitsuhashi S, Wakamatsu K, Aihara Y and Okihara N (1985) Relay using multilayer piezoelectric actuator. *Japanese Journal of Applied Physics* 24(S3): 190–192.

Rao KS, Hamza M, Kumar PA and Sravani KG (2019) Design and optimization of mems based piezoelectric actuator for drug delivery systems. *Microsystem Technologies* : 1–9.

Sadeghbeigi Olyaie M, Razfar MR and Wang S (2013) Reliability-based topology optimization design of a linear piezoelectric micromotor using an optimum finite element method. *Proceedings of the Institution of Mechanical Engineers, Part O: Journal of Risk and Reliability* 227(6): 586–598.

Santosh TV, Saraf RK, Ghosh AK and Kushwaha HS (2006) Optimum step length selection rule in modified hlcrf method for structural reliability. *International Journal of Pressure Vessels & Piping* 83(10): 742–748.

Schlinquer T, Homayouni-Amlashi A, Rakotondrabe M and Ousaid AM (2020) Design of piezoelectric actuators by optimizing the electrodes topology. *IEEE Robotics and Automation Letters* 6(1): 72–79.

Seong S, Hu C and Lee S (2017) Design under uncertainty for reliable power generation of piezoelectric energy harvester. *Journal of Intelligent Material Systems and Structures* 28(17): 2437–2449.

Sigmund O (2001) A 99 line topology optimization code written in matlab. *Structural and multidisciplinary optimization* 21(2): 120–127.

Silva E (1999) Design of piezocomposite materials and piezoelectric transducers using topology optimizationłpart ii. *Archives of Computational Methods in Engineering* 6(2): 117–182.

Silva ECN (2003) Topology optimization applied to the design of linear piezoelectric motors. *Journal of intelligent material systems and structures* 14(4-5): 309–322.

Silva EN, Fonseca JO and Kikuchi N (1997) Optimal design of piezoelectric microstructures. *Computational mechanics* 19(5): 397–410.

Silva EN, Nishiwaki S and Kikuchi N (2000) Topology optimization design of flextensional actuators. *IEEE Transactions on Ultrasonics, Ferroelectrics, and Frequency Control* 47(3): 657–671.

Stöppler G and Douglas S (2008) Adaptronic gantry machine tool with piezoelectric actuator for active error compensation of structural oscillations at the tool centre point. *Mechatronics* 18(8): 426–433.

Suleman A and Gonicalves M (1999) Multi-objective optimization of an adaptive composite beam using the physical programming approach. *Journal of intelligent material systems and structures* 10(1): 56–70.

Wan L, Chen H, Ouyang L and Chen Y (2020) A new ensemble modeling approach for reliability-based design optimization of flexure-based bridge-type amplification mechanisms. *The International Journal of Advanced Manufacturing Technology* 106(1): 47–63.

Wang L, Liang J, Chen W and Qiu Z (2019) A nonprobabilistic reliability–based topology optimization method of compliant mechanisms with interval uncertainties. *International Journal for Numerical Methods in Engineering* 119(13): 1419–1438.

Wang Y, Luo Z, Zhang X and Kang Z (2014) Topological design of compliant smart structures with embedded movable actuators. *Smart Materials and Structures* 23(4): 045024.

Youn BD, Choi KK and Du L (2005) Enriched performance measure approach for reliability-based design optimization. *AIAA journal* 43(4): 874–884.

Zhang X and Ouyang G (2008) A level set method for reliability-based topology optimization of compliant mechanisms. *Science in China Series E: Technological Sciences* 51(4): 443–455.

Zheng B, Chang CJ and Gea HC (2007) Design of piezoelectric actuator with in-plane motion using topology optimization. In: *International Design Engineering Technical Conferences and Computers and Information in Engineering Conference*, volume 48078. pp. 1343–1350.

Zheng B, Chang CJ and Gea HC (2009) Topology optimization of energy harvesting devices using piezoelectric materials. *Structural and Multidisciplinary Optimization* 38(1): 17–23.